# Dynamics of a Few Corotating Vortices in Bose-Einstein Condensates

R. Navarro, R. Carretero-González, P. J. Torres, P. G. Kevrekidis, D. J. Frantzeskakis, M. W. Ray, E. Altuntaş, and D. S. Hall

# Dynamics of Few Co-rotating Vortices in Bose-Einstein Condensates

R. Navarro[1], R. Carretero-González[1], P.J. Torres[2], P.G. Kevrekidis[3],
D.J. Frantzeskakis[4], M.W. Ray[5], E. Altuntaş[5,6], and D.S. Hall[5]

[1]*Nonlinear Dynamical Systems Group, Computational Science Research Center,*
*and Department of Mathematics and Statistics, San Diego State University, San Diego, CA 92182-7720, USA*
[2]*Departamento de Matemática Aplicada, Universidad de Granada, 18071 Granada, Spain*
[3] *Department of Mathematics and Statistics, University of Massachusetts, Amherst MA 01003-4515, USA*
[4] *Department of Physics, University of Athens, Panepistimiopolis, Zografos, Athens 157 84, Greece*
[5] *Department of Physics, Amherst College, Amherst, Massachusetts, 01002-5000 USA*
[6]*Present address: Department of Physics, Yale University, New Haven, CT 06520 USA*

We study the dynamics of small vortex clusters with few (2–4) co-rotating vortices in Bose-Einstein condensates by means of experiments, numerical computations, and theoretical analysis. All of these approaches corroborate the counter-intuitive presence of a dynamical instability of symmetric vortex configurations. The instability arises as a pitchfork bifurcation at sufficiently large values of the angular momentum that induces the emergence and stabilization of *asymmetric* rotating vortex configurations. The latter are quantified in the theoretical model and observed in the experiments. The dynamics is explored both for the integrable two-vortex system, where a reduction of the phase space of the system provides valuable insight, as well as for the non-integrable three- (or more) vortex case, which additionally admits the possibility of chaotic trajectories.

*Introduction.* The realm of atomic Bose-Einstein condensates (BECs) [1] has offered a pristine setting for studies on the dynamics of few-vortex clusters [2]. Most investigations, however, have focused on either a single vortex or large scale vortex lattices [3–6]. Recently, theoretical investigations on the study of clusters of 2–4 vortices [7–15], have appeared, chiefly motivated by the experimental realizations of such states [16–19]. This focus has heretofore centered on the fundamental building block of the vortex dipole, i.e., a pair of counter-rotating vortices.

Our aim in the present work is to explore the dynamics of small vortex clusters of 2–4 co-rotating (same charge) vortices. The original work of Ref. [2] and subsequent efforts [20] have already paved the way for an understanding of symmetric few-vortex configurations rotating as a rigid body, and their three-dimensional generalizations, e.g., U- and S-shaped vortices, and vortex rings [21]. In this context, our work presents a rather unexpected twist: we have found that the usual symmetric co-rotating vortex configurations (centered line, triangle, and square) may become *dynamically unstable*. Specifically, these states become subject to symmetry breaking, pitchfork bifurcations that lead to the spontaneous emergence of *stable asymmetric rotating vortex clusters.*

We present our analysis of these features in the integrable (at the reduced particle level) setting of a co-rotating vortex pair, and illustrate their generality by further considering a rigidly rotating vortex triplet and quadruplet. In the first case, we devise a theoretical formulation that not only explores the instability and its growth rate, but also enables a visualization of a two-dimensional reduced phase space of the system in which the pitchfork bifurcation becomes transparent. In the latter cases, we suitably parametrize the system, exploring the different regimes of symmetric and asymmetric periodic orbits. Our theoretical analysis treats vortices as classical particles, with dynamics governed by ordinary differential equations (ODEs). This reduction of the original vortex cluster system allows for the analytical characterization, numerical observation and experimental confirmation of the symmetry breaking phenomena.

*Theoretical Analysis.* As shown in Refs. [15, 19], and justified by means of a variational approximation [22], vortex dynamics governed by the two-dimensional mean-field Gross-Pitaevskii (GP) equation,

$$i\partial_t\psi = -\frac{1}{2}\Delta\psi + \frac{1}{2}\Omega^2(x^2 + y^2)\psi + |\psi|^2\psi, \qquad (1)$$

can be reduced to a system of ODEs for the vortex positions. In the original model (1), time and positions are measured, respectively, in units of $\omega_z^{-1}$ and the harmonic oscillator length along the $z$-direction, and $\Omega = \omega_x/\omega_z = \omega_y/\omega_z$, with $\omega_j$ being the harmonic trap frequency along the $j$-direction [4]. This ODE reduction is the starting point for our analysis.

The dynamics of vortex $m$ at position $(x_m, y_m)$ arises from two contributions: (i) a position-dependent vortex precession about the trap center with frequency $S_m \omega_{\mathrm{pr}}$, and (ii) a vortex-vortex interaction with vortex $n$ that induces a velocity perpendicular to their line of sight of magnitude $S_n \omega_{\mathrm{vort}}/\rho_{mn}^2$, where $\rho_{mn}$ is the distance between vortices $m$ and $n$, $S_m$ and $S_n$ are their respective charges, and $\omega_{\mathrm{vort}}$ is a dimensionless constant; see Ref. [15, 19]. The equations governing the dynamics of $N$ interacting vortices embedded in a BEC are therefore

$$
\begin{aligned}
\dot{x}_m &= -S_m\omega_{\mathrm{pr}}y_m - \frac{\omega_{\mathrm{vort}}}{2}\sum_{n\neq m}S_n\frac{y_m - y_n}{\rho_{mn}^2}, \\
\dot{y}_m &= \phantom{-}S_m\omega_{\mathrm{pr}}x_m + \frac{\omega_{\mathrm{vort}}}{2}\sum_{n\neq m}S_n\frac{x_m - x_n}{\rho_{mn}^2}.
\end{aligned}
\qquad (2)
$$

The precession about the trap center can be approximated by $\omega_{\mathrm{pr}} = \omega_{\mathrm{pr}}^0/(1 - r^2/R_{\mathrm{TF}}^2)$, where the frequency at the trap center is $\omega_{\mathrm{pr}}^0 = \ln\left(A\frac{\mu}{\Omega}\right)/R_{\mathrm{TF}}^2$, $\mu$ is the chemical potential, $R_{\mathrm{TF}} = \sqrt{2\mu}/\Omega$ is the Thomas-Fermi (TF) radius, and $A$ is a numerical constant [3, 15, 19]. To describe better the actual vortex dynamics in the trap, the constant $\omega_{\mathrm{vort}}$ in Eqs. (2) may be adjusted to account for the screening of vortex interactions due to the background density modulation [23].

We now focus on the co-rotating vortex ($S_1 = S_2 = 1$) pair. We proceed to adimensionalize Eqs. (2) by scaling $(x, y)$ by $R_{\mathrm{TF}}$ and time by $1/\omega_{\mathrm{pr}}^0$, and use polar coordinates $(x_n, y_n) = (r_n \cos(\theta_n), r_n \sin(\theta_n))$. Then, seeking symmetric stationary states $r_1 = r_2 = r_*$ and $\theta_1 - \theta_2 = \pi$ yields the rotation frequency for two vortices:

$$\omega_{\mathrm{orb}} = \dot\theta_1 = \dot\theta_2 = \frac{c}{2r_*^2} + \frac{1}{1 - r_*^2}, \qquad (3)$$

where $c = \frac{1}{2}(\omega_{\mathrm{vort}}/\omega_{\mathrm{pr}}^0)$ yields a measure of the relative strength of vortex interaction and spatial inhomogeneity. The comparison of the orbital frequency between the ODE and the GP models is given in Fig. 1a. Given the rigidly rotating nature of this state, consideration of $\delta_{mn} = \theta_m - \theta_n$ renders this state a stationary one; linearizing around it using $r_m = r_* + R_m$ and $\delta_{mn} = \pi + \delta_m$ yields the following equations of motion for the perturbations about the symmetric equilibrium:

$$\ddot R_m = -\frac{\omega_{\mathrm{ep}}^2}{2}(R_n - R_m), \quad \ddot\delta_m = -\frac{\omega_{\mathrm{ep}}^2}{2}(\delta_m - \delta_n),$$

with $\omega_{\mathrm{ep}}^2 = \frac{c^2}{2r_*^4} - \frac{2c}{(1 - r_*^2)^2}$.

It follows straightforwardly that this squared epitrochoidal (motion of a point in a circle that is rotating about another circle) relative precession frequency for two vortices *changes sign* at $r_{\mathrm{cr}}^2 = \sqrt{c}/(\sqrt{c} + 2)$. This signals our first fundamental result, namely the *destabilization* of the symmetric co-rotating vortex pair state for sufficiently large symmetric distances of the vortices from the trap center. A comparison of the ODE and GP models for the orbital and epitrochoidal precession frequencies for these two cases is given in Fig. 1a-b showing good agreement between the two. Also, by means of a numerical Bogolyubov-de-Gennes stability analysis in the rigidly rotating reference frame, we have verified that the relevant bifurcation is indeed also present in the GP model (results not shown here).

The instability of symmetric states suggests the potential existence of additional, asymmetric, ones. Seeking rigidly rotating states with $\delta_{mn} = \pi$ and $r_1^* \neq r_2^*$ yields

$$-r_1^* r_2^* (r_1^* + r_2^*)^2 + c\left(1 - r_1^{*2}\right)\left(1 - r_2^{*2}\right) = 0,$$

which will be the condition defining our radially *asymmetric* solutions. The mirror symmetry of the 2-vortex system predisposes towards the pitchfork, symmetry

breaking nature of the relevant bifurcation, a feature verified by the diagram of Fig. 1c. This diagram is given for the angle $\phi = \tan^{-1} r_2/r_1$ as a function of the angular momentum $L_0 = r_1^2 + r_2^2$, which is a conserved quantity for our system [26]. Interestingly, if the single dimensionless parameter of the system is small ($c < 3$), then the critical value $L_{\mathrm{cr}}$ for $L_0$ —at which the bifurcation from symmetric to asymmetric periodic orbits occurs— is supercritical, while if $c$ is sufficiently large ($c > 3$), it becomes subcritical [27] (not shown). Importantly, for the experimental parameters of this work, the bifurcation is supercritical and thus the asymmetric orbits generated by the symmetry breaking bifurcation are *dynamically stable*. This has been verified in the full Gross-Pitaevskii model (1), as well as in the experiments (see below).

To elucidate the pitchfork nature of the bifurcation, we develop a phase plane representation for all 2-vortex configurations. The integrability of the reduced 2-particle description can be understood on the basis of the fact that this 4-dimensional system has two integrals of motion, namely the angular momentum $L_0$, and the Hamiltonian $H$, which can be written in polar coordinates as

$$H = \frac{1}{2}\ln\left[\left(1 - r_1^2\right)\left(1 - r_2^2\right)\right] - \frac{c}{2}\ln\left[r_1^2 + r_2^2 - D\right],$$

where $D \equiv 2r_1 r_2 \cos(\delta)$ and $\delta = \theta_2 - \theta_1$. Using $L_0$ and the angle $\phi$ to express $r_1$ and $r_2$, one can rewrite the Hamiltonian as a function of $(\phi, \delta)$ thereby effectively reducing the 4-dimensional system to a 2-dimensional one. Thus, for different values of $L_0$, we can represent the orbits in the effective phase plane of $(\phi, \delta)$ in which the different orbits correspond to iso-energetic contours of constant $H(\phi, \delta)$. This is shown in Fig. 2 for values that are both below and above than the critical value of $L_0$ at fixed $c$. It can then be inferred that the symmetric fixed point with $(\phi, \delta) = (\pi/4, \pi)$ is stable in the former case, while it destabilizes in the latter case through the emergence of two additional asymmetric ($\phi \neq \pi/4$) states along the horizontal line $\delta = \pi$ of anti-diametric vortex states.

Remarkably, although the properties of the system dramatically change as we go from two vortices to three and four, the symmetry breaking bifurcation associated with the symmetric solutions persists. In particular, when $N > 2$, the persistence of the two conservation laws discussed above is not sufficient to ensure integrability of the system, and its absence is manifested in a dramatic form in the resulting 6 ($N = 3$) and 8 ($N = 4$) dimensional systems through the presence of chaotic orbits. Nevertheless, one can still analyze the highly symmetric rigidly rotating states of the system theoretically.

For $N = 3$, this state is an equilateral triangle such that $r_1 = r_2 = r_3 = r_*$ and $\delta_{i,i+1} = 2\pi/3$, with an orbital frequency predicted as $\omega_{\mathrm{orb},3} = \frac{c}{r_*^2} + \frac{1}{1 - r_*^2}$. In the rotating frame, the linear stability analysis around this rigidly rotating triangle can be performed giving rise to an epitrochoidal frequency $\omega_{\mathrm{ep},3}^2 = \frac{c^2}{r_*^4} - \frac{2c}{(1 - r_*^2)^2}$. In this
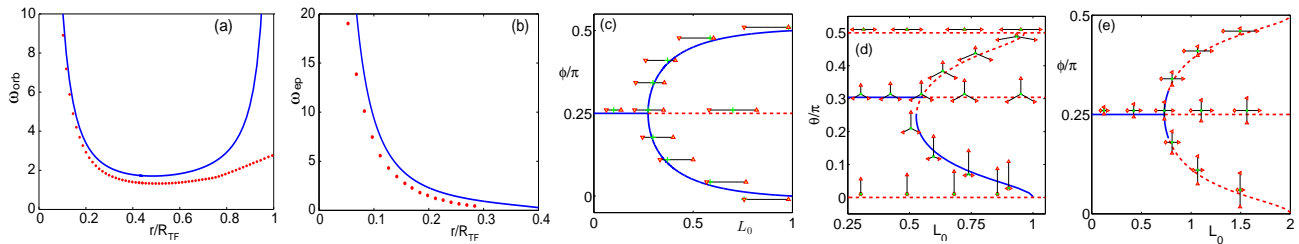
FIG. 1: (Color online) (a) Orbital and (b) epitrochoidal frequencies for two vortices vs. radial position (in rescaled units) from the center. The solid line represents results from the ODE and the dotted line from the GP model. The vanishing of the latter signals the onset of instability. Here, $\Omega = 0.05$ and $\mu = 1$. (c) Bifurcation parameter $\phi/\pi$, which equals $1/4$ when $r_1 = r_2$, vs. the square root of the angular momentum for $c = 0.1$. Panels (d) and (e) depict the corresponding phenomena for $N = 3$ and $N = 4$ vortices for $c = 0.1$. Panels (c), (d) and (e) include a few configurations along the main bifurcation branches ([blue] solid and [red] dashed lines corresponding, respectively, to stable and unstable configurations) depicting the relative position of the vortices (red triangles) with respect to the center of the condensate (green crosses).
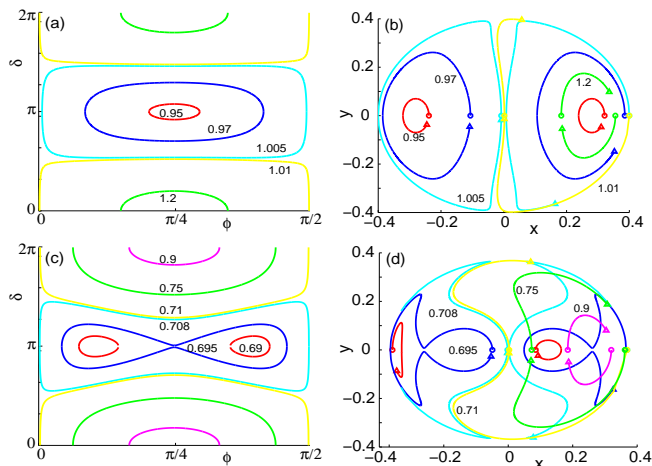


FIG. 2: (Color online) (a) Contours from the reduced Hamiltonian for vortices close to the center of the trap, i.e. $L_0 = 0.16$ below critical ($L_0 < L_{cr} = 0.273$), and (b) their respective orbits in the rotating frame defined by the symmetric configuration. Panels (c) and (d) depict, respectively, the same quantities but for vortices further out from the center for $L_0 = 0.36$ above critical ($L_0 > L_{cr} = 0.273$). The circles and triangles correspond, respectively, to the initial and final positions of the two vortices. Each color on the contour plot matches the corresponding orbit in the position diagram. Here, $c = 0.1$.

case too, a critical radius exists $r_{cr,3}^2 = \sqrt{c}/(\sqrt{c} + \sqrt{2})$, such that the symmetric state is destabilized and stable asymmetric orbits arise past this critical point, as can be seen in Fig. 1d. The dynamical picture is considerably more complicated but the conservation of the angular momentum ensures that the dynamical evolution resides on the surface of a Bloch sphere. We thus define two angular variables, $\tan\phi = r_2/r_1$ and $\cos\theta = r_3/\sqrt{L_0}$, and depict the associated pitchfork bifurcation in Fig. 1d for the subspace of solutions constrained to $r_1 = r_2$ and $\delta_{12} = \delta_{23}$. This bifurcation diagram describes a vortex configuration containing a stable symmetric rotating triangle before the bifurcation and stable asymmetric rotating triangles after the bifurcation. In addition to

the equilibrium and near-equilibrium orbits, we observe chaotic orbits arising both in a more localized form, exploring the vicinity of equilibrium orbits, and in a more extended one spanning all space (not shown).

While the general phenomena for $N = 4$ are already rather complex, some basic features can still be inferred and the symmetry breaking nature of the proposed instability persists —cf. Fig. 1e. Here, $\phi = \tan^{-1} r_3/r_1$, and we have constrained the vortices to be in a cross with right angles and $r_1 = r_3$ and $r_2 = r_4$. A general expression for the orbital frequency of the rigidly rotating state is $\omega_{orb,N} = \frac{(N-1)c}{2r_*^2} + \frac{1}{1-r_*^2}$, which is valid for any $N$. In the case of the square configuration with $r_i = r_*$ and $\delta_{i,i+1} = \pi/2$, there emerge two epitrochoidal vibrational motions with frequencies $\sqrt{-\lambda_1}$ and $\sqrt{-\lambda_2}$, where $\lambda_1 = \frac{3c}{(1-r_*^2)^2} - \frac{9c^2}{4r_*^4}$, and $\lambda_2 = \frac{4c}{(1-r_*^2)^2} - \frac{2c^2}{r_*^4}$. These, in turn, correspond to two critical points: one identical to the one given above for the $N = 3$ case, and one that is always higher, given by $r_{cr,4}^2 = \sqrt{3c}/(\sqrt{3c} + 2)$; hence, the same phenomenology persists.

*Experimental Observations.* We now discuss experimental manifestations of the symmetry breaking bifurcation and the emergence of asymmetric configurations.

The details of the experimental setup are described in Refs. [17, 19]. We begin with a magnetically-trapped BEC of $N \sim 5$–$8 \times 10^5$ atoms in the $|F = 1, m_F = -1\rangle$ hyperfine level of $^{87}$Rb. The radial and axial trap frequencies are $(\omega_r, \omega_z)/2\pi = (35.8, 101.2)$ Hz. Vortices are introduced through a process of elliptical magnetic trap distortion and rotation [24] during evaporation [25]. In terms of the trap frequencies along the major and minor axes of the distorted potential, $\omega_x$ and $\omega_y$ respectively, an ellipticity $\epsilon = (\omega_x^2 - \omega_y^2)/(\omega_x^2 + \omega_y^2) = 0.20$ and a rotation frequency of $8.5$ Hz usually produces a co-rotating pair. Higher rotation frequencies are used to generate larger numbers of co-circulating vortices.

A partial-transfer (5%) imaging method [17] is employed to create a sequence of density profiles, as shown in Fig. 3a–d. The effect of the extractions is primarily to

diminish the number of atoms in the condensate [14, 17]. Atomic losses have little effect on the parameter $c$, which scales only as $\log N$; thus $c$ falls between 0.11 and 0.10 over the range $N = 0.3$–$0.8 \times 10^6$ atoms. For convenience, we take $c = 0.1$ in the following analysis.

We examine 52 experimental time series consisting of 8 snapshots spanning 240 to 480 ms. For each snapshot the vortex centers and the radius of the cloud are extracted using least squares fitting (see panels a–d in Fig. 3). The vortex positions are then normalized to the BEC radius (i.e., TF units) and the angular momentum $L_0$ and Hamiltonian $H$ are computed for each frame (panels e–h in Fig. 3). For each series, the average angular momentum $\overline{L}_0$ and Hamiltonian $\overline{H}$ are determined (horizontal dashed lines in the middle panels in Fig. 3). Using $\overline{L}_0$ we compare the experimental points representing each orbit in the $(\phi, \delta)$ plane to the isocontour of $H$ corresponding to $\overline{H}$, as shown in the right column of panels in Fig. 3, finding good agreement between the two.

Panels a–d in Fig. 3 depict typical time series, together with their respective fits, that exemplify the different qualitative cases that we observed in the experiments. In particular, the vortex dynamics depends on whether the average angular momentum is below or above the critical threshold $L_{\mathrm{cr}} = 2r_{\mathrm{cr}}^2$. This distinguishes cases in which asymmetric orbits are, respectively, non-existent and possible. The different qualitative cases that we observe may be grouped as follows:

• For $\overline{L}_0 < L_{\mathrm{cr}}$ and relatively small $\overline{H}$, the experiment displays *symmetric* orbits (rows a and e in Fig. 3).

• For $\overline{L}_0 > L_{\mathrm{cr}}$ and moderate $\overline{H}$, the experiment displays (i) orbits where both vortices (in the rigidly rotating frame) are approximately on the *same* side of the cloud chasing each other on the same path (rows b and f in Fig. 3) or (ii) *asymmetric* orbits (rows c and g in Fig. 3). The particular class of orbit is determined by the initial conditions. Initial conditions inside the area delimited by the separatrix (red double-loop curve in the right panels of Figs. 3f and 3g) emanating from the saddle point $(\phi, \delta) = (\pi/4, \pi)$ give rise to asymmetric orbits.

• For $\overline{L}_0 > L_{\mathrm{cr}}$ and large $\overline{H}$, the experiment displays orbits in which one vortex remains close to the center while the other orbits around it close to the periphery of the cloud (rows d and h in Fig. 3).

As is clear from these examples and the remaining 48 data sets (see supplemental material), asymmetric orbits are found only when $\overline{L}_0 > L_{\mathrm{cr}}$ and when the vortex orbits fall inside the asymmetric minima regions of the Hamiltonian picture in the $(\phi, \delta)$ plane. Asymmetric solutions are absent in all of the cases for which $\overline{L}_0 < L_{\mathrm{cr}}$. These results are in good agreement with the theoretical prediction of the pitchfork bifurcation depicted in Fig. 1c. Note that some of the experimental vortex trajectories, which are measured over a fixed time interval, span only a fraction of the full period of their corresponding orbits (cf. left panel of Fig. 3f); the latter vary in duration and
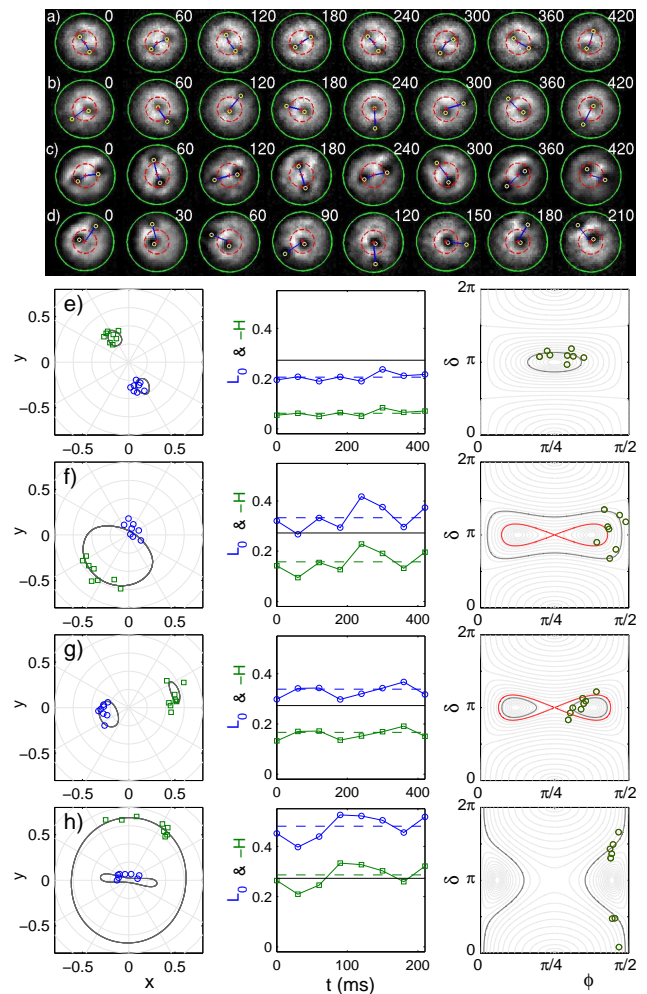


FIG. 3: (Color online) (a–d): Typical experimental series for the dynamics of two co-rotating vortices (time indicated in ms). The large (green) circles and the (red) crosses represent, respectively, the fitted TF radius and center of the cloud while the small (yellow) dots depict the fitted vortex centers. The (red) dashed circles represent the critical radius, $r_{\mathrm{cr}}$, above which symmetric orbits become unstable. (e–h): Manifestation of the pitchfork bifurcation for the experimental series depicted in panels a–d which correspond to $c = 0.1$. Left column: experimental vortex positions and their corresponding orbit from the reduced ODE model (solid line), in TF units in the rigidly rotating frame. Middle column: corresponding $L_0$ (blue circles) and $-H$ (green squares) and their averages (horizontal dashed lines) as well as the critical value for $L_0$ (solid horizontal line). Right column: corresponding orbits in the $(\phi, \delta)$ plane along with isocontours for constant $H$ (highlighted in dark gray is the isocontour corresponding to the average $H$ and in red is the separatrix delimiting the area containing asymmetric orbits).

can become quite long (e.g., close to a separatrix).

To extend our considerations, we briefly present a comparison between experiment and theory for $N = 3$ and $N = 4$ vortices. The main phenomena are depicted using two examples for each case in Fig. 4. Panels a and b correspond to the $N = 3$ vortex case below and above
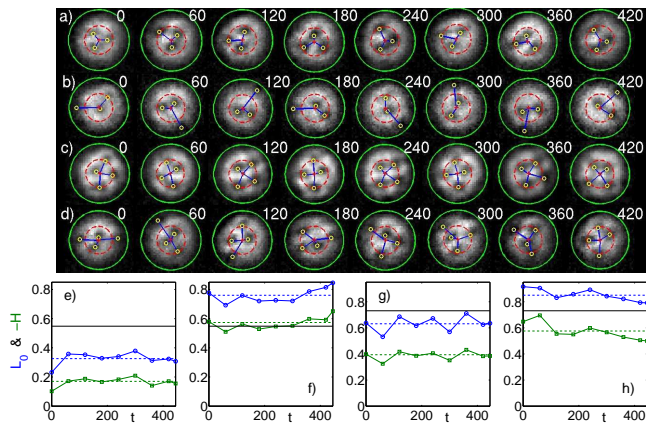
FIG. 4: (Color online) Experimental series for trios (a and b) and quartets (c and d) below (a and c) and above (b and d) the critical threshold. (e–h): Corresponding time series for $L_0$ and $-H$. Same notation and units as in Fig. 3.

the pitchfork bifurcation (see panel e and f). Panels c and d depict the equivalent scenario for $N = 4$ vortices. As the figure illustrates, and is observed in all of the cases that we studied (17 data sets for $N = 3$ and 5 data sets for $N = 4$; not shown), the main phenomenology for $N = 3$ and $N = 4$ persists in that all configurations with $\overline{L}_0 > L_{cr}$ are not symmetric, and symmetric configurations —or epitrochoidal oscillations about them— are only present when $\overline{L}_0 < L_{cr}$.

*Conclusions.* We have revisited the theme of co-rotating few vortex clusters in atomic Bose-Einstein condensates. By a combination of theoretical analysis, numerical computation and experimental observation, we have illustrated a strong manifestation of symmetry breaking through a pitchfork bifurcation, which leads to the destabilization of symmetric solidly rotating configurations and gives rise to the the emergence of *stable* rigidly rotating but *asymmetric* vortex configurations. We showed that this analysis is fruitful not only for the integrable (at the reduced particle level) two-vortex setting, where a suitable parametrization of the phase space was provided, but also for the non-integrable cases of $N = 3$ and $N = 4$ vortices where chaotic orbits exist.

Naturally, it would be interesting to provide a more global characterization of the dynamics of the three-body problem, which is perhaps the most analytically tractable and intriguing case due to its potential for chaos. Another expansion of the present considerations involves their generalization to higher dimensions. In this case, it would be interesting to see, upon gradual decrease of the trapping frequency in the third dimension, whether the symmetry-breaking phenomena persist for line vortices and vortex rings. These aspects are presently under consideration and results will be reported elsewhere.

01
02
03
04
05
06
08
09
10
11
12
13

[1] C. J. Pethick and H. Smith, *Bose-Einstein Condensation in Dilute Gases* (Cambridge University Press, Cambridge, 2002); L. Pitaevskii and S. Stringari, *Bose-Einstein Condensation* (Oxford University Press, 2003).
[2] Y. Castin and R. Dum, Eur. Phys. J. D, **7**, 399 (1999).
[3] A. L. Fetter and A. A. Svidzinsky, J. Phys.: Condens. Matter **13**, R135 (2001).
[4] P. G. Kevrekidis, D. J. Frantzeskakis and R. Carretero-González, *Emergent Nonlinear Phenomena in Bose-Einstein Condensates* (Springer-Verlag, Berlin, 2008).
[5] A. L. Fetter, Rev. Mod. Phys. **81**, 647 (2009).
[6] P. K. Newton and G. Chamoun, SIAM Review **51**, 501 (2009).
[7] L.-C. Crasovan *et al.*, Phys. Rev. E **66**, 036612 (2002).
[8] L.-C. Crasovan *et al.*, Phys. Rev. A **68**, 063609 (2003).
[9] Q. Zhou and H. Zhai, Phys. Rev. A **70**, 043619 (2004).
[10] M. Möttönen *et al.*, Phys. Rev. A **71**, 033626 (2005).
[11] V. Pietilä *et al.*, Phys. Rev. A **74**, 023603 (2006).
[12] W. Li *et al.*, Phys. Rev. A **77**, 053610 (2008).
[13] S. Middelkamp *et al.*, Phys. Rev. A **82**, 013646 (2010).
[14] P. Kuopanportti *et al.*, Phys. Rev. A **83**, 011603 (2011).
[15] P. J. Torres *et al.*, Phys. Lett. A **375**, 3044 (2011).
[16] T. W. Neely *et al.*, Phys. Rev. Lett. **104** , 160401 (2010).
[17] D. V. Freilich, *et al.*, Science, **329** (2010) 1182.
[18] J. A. Seman *et al.*, Phys. Rev. A **82**, 033616 (2010).
[19] S. Middelkamp *et al.*, Phys. Rev. A **84**, 011605(R) (2011).
[20] A. Aftalion and I. Danaila, Phys. Rev. A **68**, 023603 (2003); *ibid.* **69**, 033608 (2004); I. Danaila, *ibid.* **72**, 013605 (2005).
[21] S. Komineas, Eur. Phys. J.-Spec. Top. **147**, 133 (2007).
[22] D. E. Pelinovsky and P. G. Kevrekidis, Nonlinearity **24**, 1271 (2011).
[23] S. McEndoo and Th. Bush, Phys. Rev. A **79**, 053616 (2009).
[24] E. Hodby *et al.*, Phys. Rev. Lett. **88**, 010405 (2001).
[25] K. W. Madison *et al.*, Phys. Rev. Lett. **84**, 806 (2000).
[26] Note that $L_0$ here refers to the angular momentum carried by the vortices as used in fluid mechanics (see, e.g., Ref. [6]) rather than the (quantized) orbital angular momentum as used in quantum mechanics.
[27] The latter bifurcation is of merely mathematical interest, as for typical values of the physical parameters, the supercritical scenario is the one which is realized.